J|A|C|S ARTICLES

Published on Web 03/12/2009

# A New Ferrimagnet Based on a Radical-Substituted Radical Cation Salt

Yuki Masuda,[†] Masato Kuratsu,[†] Shuichi Suzuki,[†] Masatoshi Kozaki,[†] Daisuke Shiomi,*[,†] Kazunobu Sato,[†] Takeji Takui,[†] Yuko Hosokoshi,[‡] Xiao-Zheng Lan,[§] Yuji Miyazaki,[§] Akira Inaba,[§] and Keiji Okada*[,†]

*Department of Chemistry, Graduate School of Science, Osaka City University, Sugimoto, Sumiyoshi-ku, Osaka 558-8585, Japan, Department of Physical Science, Graduate School of Science, Osaka Prefecture University, Sakai, Osaka 599-8531, Japan, and Research Center for Molecular Thermodynamics, Graduate School of Science, Osaka University, Toyonaka, Osaka 560-0043, Japan*

Received October 16, 2008; E-mail: shiomi@sci.osaka-cu.ac.jp; okadak@sci.osaka-cu.ac.jp

***Abstract:*** Radical-substituted radical cations are attractive spin building blocks of molecule-based magnets. The introduction of an additional spin as a counteranion provides a unique three-spin system wherein the magnetic interactions between the spins of the radical substituent and the radical cation ($J_{intra}$) and those between the spins of the radical cation and the anion ($J_{inter}$) play decisive roles in determining the magnetic properties of the system. We report the first demonstration of a ferrimagnet by utilizing a large-$J_{intra}$ system, nitronyl nitroxide-substituted dihydrophenazine radical cation (**NNDPP**$^{\bullet+}$) in combination with tetrabromoferrate ($FeBr_4^-$) as the counteranion. On the basis of measurements of dc and ac magnetic susceptibilities and heat capacity, the magnetic properties of **NNDPP**$^{\bullet+}\cdot FeBr_4^-$ are elucidated to be those of a three-dimensional long-range-ordered ferrimagnet with $T_c = 6.7$ K.

## Introduction

In the last few decades, considerable developments have occurred in the field of molecule-based magnets. Various approaches to developing magnetic materials with *m*-dimensional (*m*D, $m = 1-3$) and even single-molecule (0D) spin structures have been used both experimentally and theoretically.[1] For instance, magnetic hysteresis has long been believed to be a characteristic of 3D magnets; however, recent advances have demonstrated the occurrence of magnetic hysteresis even in lower-dimensional magnets, such as single-molecule magnets (SMMs, 0D)[2] composed of clusters of metal ions with a large single-ion magnetic anisotropy. Organic radicals have also played important roles in these developments, as in the following examples: a (nitronyl nitroxide)−$Co(hfac)_2$ chain complex[3] behaves as a single-chain magnet (SCM, 1D)[4] and exhibits slow relaxation of magnetization and hysteresis effects; $C_{60}$−TDAE [TDAE = tetrakis(dimethylamino)ethylene] is a unique charge-transfer (CT) complex showing ferromagnetic-like behavior;[5] a dithiadiazolyl radical behaves as a weak ferromagnet at 36 K;[6] and a fascinating organic radical polymer ($S \approx 5000$) exhibits spin-glass-like character below 10 K.[7]

In these studies, organic spin carriers are usually radicals or radical ions in CT salts. A unique approach utilizing radical-substituted CT salts was theoretically proposed by Yamaguchi et al.[8] in order to develop new organic-based magnets. Although various studies including aniline,[9] ferrocene,[10] and TTF[9,11,12] radical cations with nitronyl nitroxide (**NN**) have been examined, no successful results have been reported to date. The difficulty in realizing this system may be due to the weakness of the magnetic interactions between the radical substituents and

[†] Osaka City University.
[‡] Osaka Prefecture University.
[§] Osaka University.

(1) (a) *Magnetism: Molecules to Materials II*−*V*; Miller, J. S., Drillon, M., Eds.; Wiley-VCH: New York, 2001−2005. (b) Gatteschi, D.; Sessoli, R.; Villain, J. In *Molecular Nanomagnets*; Oxford: New York, 2006; pp 1−395.
(2) (a) Sessoli, R.; Gatteschi, D.; Caneschi, A; Novak, M. A. *Nature* **1993**, *365*, 141–143. (b) Sessoli, R.; Tsai, H.-L.; Schake, A. R.; Wang, S.; Vincent, J. B.; Folting, K.; Gatteschi, D.; Christou, G.; Hendrickson, D. N. *J. Am. Chem. Soc.* **1993**, *115*, 1804–1816. (c) Gatteschi, D.; Sessoli, R. *Angew. Chem., Int. Ed.* **2003**, *42*, 268–297.
(3) Caneschi, A.; Gatteschi, D.; Lalioti, N.; Sangregorio, C.; Sessoli, R.; Venturi, G.; Vindigni, A.; Rettori, A.; Pini, M. G.; Novak, M. A. *Angew. Chem., Int. Ed.* **2001**, *40*, 1760–1763.
(4) Clérak, R.; Miyasaka, H.; Yamashita, M.; Coulson, C. *J. Am. Chem. Soc.* **2002**, *124*, 12837–12844.
(5) Allemand, P.-M.; Khemani, K. C.; Koch, A.; Wudl, F.; Holczer, K.; Donovan, S.; Grüner, G.; Thompson, J. D. *Science* **1991**, *253*, 301–303.
(6) Banister, A.; Bricklebank, N.; Lavender, I.; Rawson, J. M.; Gregory, C. I.; Tanner, B. K.; Clegg, W.; Elsegood, M. R. J.; Palacio, F. *Angew. Chem., Int. Ed.* **1996**, *35*, 2532–2535.
(7) Rajca, A.; Wongsriratanakul, J.; Rajca, S. *Science* **2001**, *294*, 1503–1505.
(8) Yamaguchi, K.; Namimoto, H.; Fueno, T. *Chem. Phys. Lett.* **1990**, *166*, 408–414.
(9) (a) Sugano, T.; Fukasawa, T.; Kinoshita, M. *Synth. Met.* **1991**, *41*−*43*, 3281–3284. (b) Sakurai, H.; Izuoka, A.; Sugawara, T. *J. Am. Chem. Soc.* **2000**, *122*, 9723–9734.
(10) Nakamura, Y.; Koga, N.; Iwamura, H. *Chem. Lett.* **1991**, *20*, 69–72.
(11) (a) Matsushita, M. M.; Kawakami, H.; Kawada, Y.; Sugawara, T. *Chem. Lett.* **2007**, *36*, 110–111. (b) Nakazaki, J.; Ishikawa, Y.; Izuoka, A.; Sugawara, T.; Kawada, Y. *Chem. Phys. Lett.* **2000**, *319*, 385–390. (c) Kumai, R.; Matsushita, M. M.; Izuoka, A.; Sugawara, T. *J. Am. Chem. Soc.* **1994**, *116*, 4523–4524.
(12) (a) Sugimoto, T.; Yamaga, S.; Nakai, M.; Ohmori, K.; Tsuji, M.; Nakatsuji, H.; Fujita, H.; Yamauchi, J. *Chem. Lett.* **1993**, *22*, 1361–1364. (b) Sugimoto, T.; Yamaga, S.; Nakai, M.; Tsuji, M.; Nakatsuji, H.; Hosoito, N. *Chem. Lett.* **1993**, *22*, 1817–1820.

 **10.1021/ja808093z CCC: $40.75** 

radical cations ($J_{intra}$) in comparison with the relatively large antiferromagnetic interactions in CT salts (typical values for CT magnetic interactions are $J_{inter}/k_B = -100$ to $-1000$ K, where $\hat{H} = -2J_{inter}\hat{S}_D \cdot \hat{S}_A$).[13] When $|J_{inter}| \gg |J_{intra}|$, the system behaves like a radical-substituted diamagnetic ion pair at low temperature, resulting in paramagnetic behavior, as has been observed.[9a,12b] To realize the proposed system, a relatively large value of $J_{intra}$ seems to be essential. Therefore, we have recently developed several $\pi$-donor systems applicable to this approach.[14] Of these, 2-**NN**-5,10-dihydro-5,10-diphenylphenazine radical cation (**NNDPP**$^{\bullet+}$) seems to be an attractive framework.[14a] Here we report the development of the first ferrimagnet based on the radical-substituted radical cation salt, **NNDPP**$^{\bullet+}\cdot FeBr_4^-$, which consists of three unique heterospins: the **NN**, **DPP**$^{\bullet+}$, and Fe(III) spins.

## Experimental Section

**Experimental Methods.** X-ray data were collected at 93 K using a Rigaku CCD area detector with graphite-monochromatized Mo Kα radiation. The structure was solved by a direct method (*SIR92*) and expanded using a Fourier technique. All of the calculations were performed using the *Crystal Structure* crystallographic software package. The magnetic measurements were performed using a Quantum Design MPMS-XL SQUID magnetometer for randomly oriented polycrystalline samples. The dc magnetizations were measured over the temperature range 1.9−298 K in static magnetic fields of up to 7 T. The ac susceptibilities were measured below 15 K under ac fields of 3 Oe with frequencies of 0.01−1000 Hz. The heat capacity measurements were carried out with a Quantum Design PPMS 6000 relaxation-type calorimeter.

**Preparation of Thianthrene$^{\bullet+}\cdot FeBr_4^-$.** The oxidation of thianthrene was carried out in an electrochemical cell under conditions similar to those for the $FeCl_4^-$ salt described in our previous paper.[15] An electrolyte solution of tetra-*n*-butylammonium tetrabromoferrate (1.32 g, 2.14 mmol) in dry dichloromethane (50 cm$^3$) was prepared. Half of the solution was added to the cathodic compartment in the cell. Thianthrene (381 mg, 1.76 mmol) was dissolved in the remaining electrolyte solution, which was then added to the anodic compartment. Both compartments in the cell were purged with argon for 10 min. The electrolysis was carried out at constant current (1.0 mA) using a galvanostat. After 1 day, black powder was deposited on the Pt surface. The powder was collected several times (647 mg, 62% after three cycles). The prepared thianthrene$^{\bullet+}\cdot FeBr_4^-$ was sufficiently pure, as confirmed by elemental analysis. Analytical data for thiathrene$^{\bullet+}\cdot FeBr_4^-$ ($C_{12}H_8Br_4FeS_2$, fw 591.78): Black powder; mp ∼204 °C (dec). MS: (FAB$^+$), *m/z* 216 [$C_{12}H_8S_2^{\bullet+}$]; (FAB$^-$), *m/z* 376 [$FeBr_4^-$]. IR (KBr, cm$^{-1}$): 1541, 1518, 1452, 1439, 1431, 1418, 1304, 1261, 1150, 1101, 1026, 762, 752, 660. Anal. Calcd for $C_{12}H_8Br_4FeS_2$: C, 24.35; H, 1.36. Found: C, 24.35; H, 1.28. EPR (powder): $g = 2.0438$ as a broad and monotonic signal with a width of 540 G at half-height.

**Preparation of NNDPP$^{\bullet+}\cdot FeBr_4^-$.** The chemical oxidation of neutral **NNDPP** was carried out using dry solvents in a glovebox as follows. A solution of thianthrene$^{\bullet+}\cdot FeBr_4^-$ (48 mg) in acetonitrile (20 cm$^3$) was added at room temperature to a solution of neutral **NNDPP** (40 mg) in dichloromethane (5 cm$^3$). The reaction mixture was stirred for 30 min and then filtered through a syringe filter (DISMIC-25, pore size 0.50 μm) to remove trace amounts of insoluble materials, if any. The filtrate was evaporated under reduced pressure. The residue was dissolved in a minimum amount of dichloromethane (∼10 cm$^3$). An excess amount of diethyl ether (∼30 cm$^3$) was added to the dichloromethane solution, giving crude **NNDPP**$^{\bullet+}\cdot FeBr_4^-$ as a brownish precipitate. This compound was dissolved in 7 cm$^3$ of 1,2-dichloroethane in a small bottle. The uncapped bottle was placed in a larger bottle containing pentane (∼10 cm$^3$). The larger bottle was capped and kept at room temperature for 3 days, giving 40 mg of **NNDPP**$^{\bullet+}\cdot FeBr_4^-$ as dark-red prisims (57% yield). Analytical data for **NNDPP**$^{\bullet+}\cdot FeBr_4^-$ ($C_{31}H_{29}Br_4FeN_4O_2$, fw 865.05): Mp: 226 °C. MS: (FAB$^+$), *m/z* 490 [**NNDPP**$^{\bullet+}$]; (FAB$^-$), *m/z* 376 [$FeBr_4^-$]. IR (KBr, cm$^{-1}$): 3099, 1541, 1489, 1371. Anal. Calcd for $C_{31}H_{29}Br_4FeN_4O_2$: C, 43.04; H, 3.38; N, 6.48. Found: C, 43.11; H, 3.56; N, 6.47. EPR (powder): $g = 2.008$ as a sharp line for **NNDPP**$^{\bullet+}$ and 2.046 as a very broad line with a width of ∼2200 G at half-height for $FeBr_4^-$. Crystallographic data for **NNDPP**$^{\bullet+}\cdot FeBr_4^-$: monoclinic; space group $P2_1/a$; $a = 13.8094(9)$ Å, $b = 15.6034(8)$ Å, $c = 15.0910(10)$ Å, $\beta = 100.736(4)°$; $V = 3194.8(3)$ Å$^3$; $Z = 4$; $\rho_{calcd} = 1.798$ g cm$^{-3}$; $T = 93$ K; $R = 0.0443$, $R_w = 0.0670$, GOF = 1.006. The crystallographic data is given in the Supporting Information and has been deposited with the Cambridge Crystallographic Data Centre (entry no. CCDC 702019).

*Scheme 1*

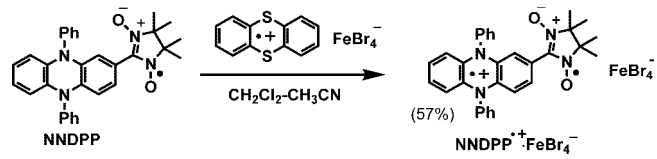


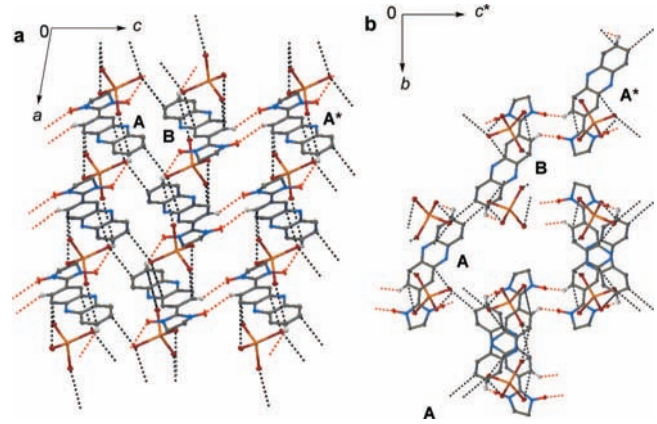


***Figure 1.*** Crystal packing structure of **NNDPP**$^{\bullet+}\cdot FeBr_4^-$. (a) View projected along the *b* axis. (b) View along the *a* axis. The dotted lines show short contacts (black lines for the Br−C contacts, red lines for the O−HC contacts). The methyl and phenyl groups and most of the hydrogen atoms have been omitted for clarity.

## Results and Discussion

**NNDPP**$^{\bullet+}\cdot FeBr_4^-$ was prepared through the chemical oxidation of neutral **NNDPP** with 1 equiv of thianthrene$^{\bullet+}\cdot FeBr_4^-$ in $CH_2Cl_2/CH_3CN$ and obtained as dark-red prisms after recrystallization (Scheme 1). **NNDPP**$^{\bullet+}\cdot FeBr_4^-$ in a crystalline or powder form is stable under aerated conditions and can be kept in a freezer for a long time.

Figure 1 shows the crystal packing structure of **NNDPP**$^{\bullet+}\cdot FeBr_4^-$. There are several short contacts between the magnetically important atoms (the Br atoms in $FeBr_4^-$, the C atoms in **DPP**$^{\bullet+}$, and the O atoms in **NN**) within or close to the sum of the van der Waals radii: the Br−C contacts (3.50−3.70 Å) and the O−HC contacts (2.57 Å for a single contact, 2.53 Å for a double contact, see Figure 1). The Br−C contacts are most likely to induce an antiferromagnetic interaction between

(13) Nordio, P. L.; Soos, Z. G.; McConnell, H. M. *Annu. Rev. Phys. Chem.* **1966**, *17*, 237–260.
(14) (a) Hiraoka, S.; Okamoto, T.; Kozaki, M.; Shiomi, D.; Sato, K.; Takui, T.; Okada, K. *J. Am. Chem. Soc.* **2004**, *126*, 58–59. (b) Kuratsu, M.; Kozaki, M.; Okada, K. *Angew. Chem., Int. Ed.* **2005**, *44*, 4056–4058.
(15) Kuratsu, M.; Suzuki, S.; Kozaki, M.; Shiomi, D.; Sato, K.; Takui, T.; Okada, K. *Inorg. Chem.* **2007**, *46*, 10153–10157.

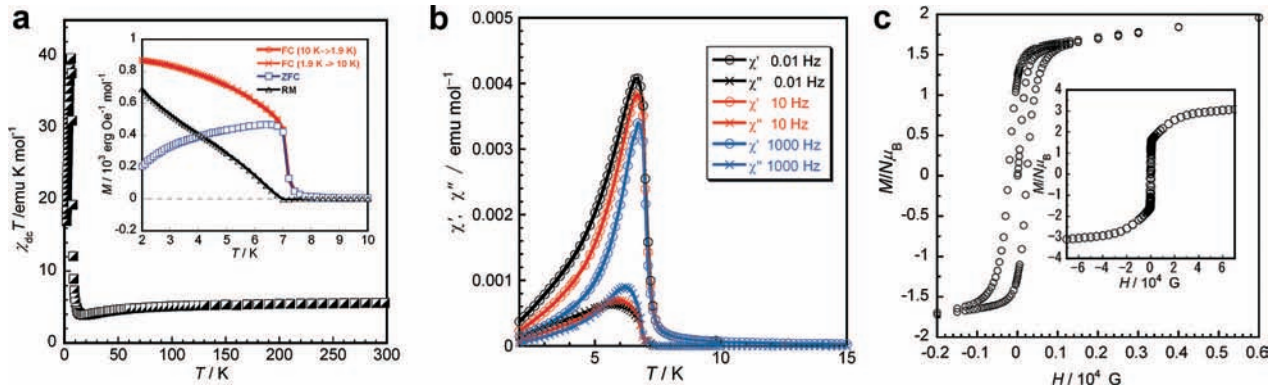


***Figure 2.*** Magnetic properties of **NNDPP**$^{\bullet+}$·$FeBr_4^-$. (a) Temperature dependence of $\chi_{dc}T$ under a static field of 1000 Oe. Inset: temperature dependence of the magnetization under FC and ZFC conditions and the remnant magnetization (RM) under 10 Oe. (b) Temperature dependence of the real ($\chi'$) and imaginary ($\chi''$) parts of the ac susceptibility. The solid lines are guides to the eye. (c) $M(H)$ curve at 1.9 K in a region of low magnetic field. Inset: $M(H)$ curve in a region of higher magnetic field.

the $\pi$-radical cation and the Fe(III) spins,[16] whereas the O−HC contacts would induce a ferromagnetic interaction between the adjacent **NNDPP**$^{\bullet+}$ moieties, as can be deduced from the theoretical calculations on model systems I and II (see the Supporting Information). The Br−C contacts not only extend in the *a* direction but also bridge the *c*-directed nearest-neighbor **NNDPP**$^{\bullet+}$ moieties (**A** and **B** in Figure 1a) through $FeBr_4^-$, making a double-chain structure, $2(-FeBr_4^- - \mathbf{NNDPP}^{\bullet+}-)_n$, extending in the *a* direction. The O−HC contacts within the double chain (model I in the Supporting Information) cooperatively function with the Br−C contacts to induce a ferrimagnetic spin alignment. In addition, the **NNDPP**$^{\bullet+}$ moieties in adjacent double chains (**B** and **A*** in Figure 1a) are connected by the two O−HC contacts, which would induce a ferromagnetic interaction between **B** and **A*** in the *ac* plane (model II in the Supporting Information). The similar combination of the Br−C and O−HC contacts is also observed along the *b* direction. Thus, a 3D-type spin alignment is expected for **NNDPP**$^{\bullet+}$·$FeBr_4^-$.

The temperature dependence of $\chi_{dc}T$ (where $\chi_{dc}$ is the dc magnetic susceptibility) is shown in Figure 2a. The $\chi_{dc}T$ value at room temperature is 5.61 emu K mol$^{-1}$, which is close to the theoretical value (5.59 emu K mol$^{-1}$ using $g = 2.008$ for **NNDPP**$^{\bullet+}$ and $g = 2.046$ for $FeBr_4^-$ from powder EPR) for $S = {}^5/_2$ [Fe(III)] plus $S = 1$ (**NNDPP**$^{\bullet+}$) and compatible with a strongly ferromagnetic interaction between the **NN** and **DPP**$^{\bullet+}$ moieties.[14a] As the temperature decreases, $\chi_{dc}T$ gradually decreases to a minimum value (3.93 emu K mol$^{-1}$ at 18 K) and then sharply increases below 18 K, reflecting a ferrimagnetic spin alignment. Furthermore, $\chi_{dc}T$ reaches a maximum value (39.67 emu K mol$^{-1}$) at ~6 K and sharply drops at lower temperatures. In order to obtain insight into the sharp drop below 6 K, experiments were performed under field-cooled (FC) and zero-field-cooled (ZFC) conditions. The $M(T)$ curves split sharply at 7.0 K, and the remnant magnetization disappears in the same temperature region (Figure 2a, inset). These results suggest the onset of a phase transition into a ferrimagnetically ordered state at $T_c = 6.7$ K (from heat capacity measurements, as described below).

The ac susceptibility was measured at a zero static field with a weak ac field (3 Oe) (Figure 2b). The real component, $\chi'(T)$, shows a clear peak maximum at 6.7 K that is frequency-independent, suggesting a negligible contribution of spin-glass character.[17] This behavior is obviously different from that of low-dimensional magnets such as SMMs and SCMs. The imaginary component, $\chi''(T)$, exhibits a broader peak in the same temperature region that suggests net magnetization without an external field.[18] Interestingly, the shape of the broad peak is frequency-dependent [with a peak temperature of 5.7 K (0.01 Hz) to 6.2 K (1000 Hz)]. Such a difference in the behaviors of $\chi'(T)$ and $\chi''(T)$ has been observed for some ferromagnetic systems.[19] The frequency-dependent $\chi''(T)$ would be related to energy losses of the dynamic behavior of domain-wall movement and/or domain magnetization rotation induced by the ac magnetic field.

In accordance with these results, magnetic hysteresis was observed at 1.9 K with a remnant magnetization of $M_R = 1.2\ N\mu_B$ and a coercive field of 230 Oe (Figure 2c). The magnetization curve $M(H)$ saturates under the higher field, ~7 T. The saturation magnetization value ($M_S = 3.08\ N\mu_B$) is in good agreement with the theoretical value ($M_S = g\mu_B\Delta S = 3.05\ N\mu_B$) with $\Delta S = ({}^5/_2 - 1)$, indicating a phase transition into a ferrimagnet. The fact that the $M_R$ value is smaller than the $M_S$ value is due to the magnetocrystalline anisotropy, as frequently observed in ferrimagnetic molecular systems.[20]

In order to elucidate the mechanism of the magnetic phase transition of **NNDPP**$^{\bullet+}$·$FeBr_4^-$ in more detail, the heat capacities were measured under various magnetic fields by the relaxation method. Figure 3 shows the heat capacities $C_p$ and magnetic heat capacities $C_{mag}$ of **NNDPP**$^{\bullet+}$·$FeBr_4^-$ as functions of temperature under various magnetic fields. To determine $C_{mag}$, the lattice heat capacity was evaluated by fitting the $C_p$ data at zero magnetic field between 15 and 20 K to the following equation: $C_p = aT^3 + bT^5 + cT^7 + dT^9 + eT^{-2}$, where the first four terms represent the lattice heat capacity[21] and the last term corresponds to a contribution from the short-range-order effect

(16) Miyazaki, A.; Enomoto, M.; Enomoto, M.; Enoki, T.; Saito, G. *Mol. Cryst. Liq. Cryst.* **1997**, *305*, 425–434.
(17) Midosh, J. A. In *Spin Glasses: An Experimental Introduction*; Taylor & Francis: London, 1993; pp 45−117.
(18) Palacio, F.; Lazard, F. J.; van Duyneveldt, A. J. *Mol. Cryst. Liq. Cryst.* **1989**, *176*, 289–305.
(19) Levin, E. M.; Pecharsky, V. K.; Gschneidner, K. A., Jr. *J. Appl. Phys.* **2001**, *12*, 6255–6262.
(20) (a) Inoue, K.; Hayamizu, T.; Iwamura, H.; Hashizume, D.; Ohashi, Y. *J. Am. Chem. Soc.* **1996**, *118*, 1803–1804. (b) Kahn, O.; Pei, Y.; Verdaguer, M.; Renard, J. P.; Sletten, J. *J. Am. Chem. Soc.* **1988**, *110*, 782–789.
(21) Miyazaki, Y.; Matsumoto, T.; Ishida, T.; Nogami, T.; Sorai, M. *Bull. Chem. Soc. Jpn.* **2000**, *73*, 67–71.

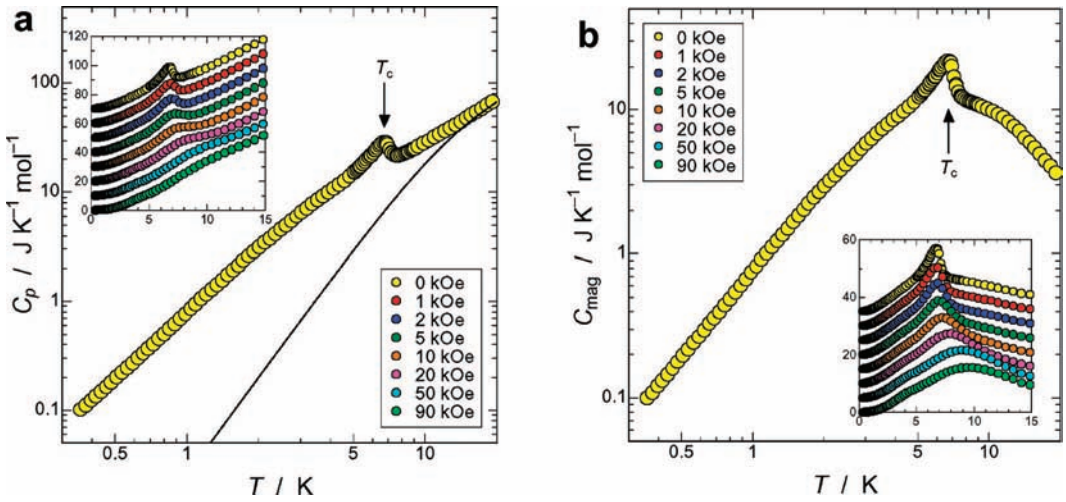


***Figure 3.*** Heat capacities $C_p(T)$ and magnetic heat capacities $C_{mag}(T)$ of **NNDPP**$^{\bullet+}$·$FeBr_4^-$ as functions of temperature under various magnetic fields. (a) $C_p(T)$ with an estimated curve of the heat capacity $C_{lat}(T)$ due to lattice contribution (solid line). Inset: magnetic field dependence of $C_p(T)$. (b) Temperature dependence of $C_{mag} = C_p - C_{lat}$. Inset: magnetic field dependence of $C_{mag}(T)$. In the insets, the $y$ axis shows only a relative scale to compare the peak positions under the magnetic fields.

of the spin alignment.[22] The values of the constants obtained from the fit were $a = 2.547 \times 10^{-2}$ J K$^{-4}$ mol$^{-1}$, $b = -8.517 \times 10^{-5}$ J K$^{-6}$ mol$^{-1}$, $c = 1.478 \times 10^{-7}$ J K$^{-8}$ mol$^{-1}$, $d = -1.025 \times 10^{-10}$ J K$^{-10}$ mol$^{-1}$, and $e = 1.338 \times 10^{3}$ J K mol$^{-1}$. The $C_{mag}$ data were then obtained by subtracting the lattice contribution ($C_{lat} = aT^3 + bT^5 + cT^7 + dT^9$, shown as the solid curve in Figure 3a) from the total heat capacities.

A heat capacity peak due to the phase transition was observed at $T_c = 6.7$ K at zero magnetic field. As the magnetic field increased, this peak shifted to higher temperatures and broadened. This behavior is typical for ferromagnetic[23] and/or ferrimagnetic systems.[24] Furthermore, a heat capacity hump was observed above $T_c$, which is a characteristic of low-dimensional magnetic systems.

The magnetic entropy at zero magnetic field was evaluated to be 23.8 J K$^{-1}$ mol$^{-1}$. This value agrees well with the value expected for a spin system composed of $S = 1$ (**NNDPP**$^{\bullet+}$) and $S = {}^5/_2$ [Fe(III)], which is given by $R$ ln(3 × 6) = 24.0 J K$^{-1}$mol$^{-1}$.

In summary, the results from the magnetic susceptibility and heat capacity measurements are entirely consistent with the proposed 3D ferrimagnet below $T_c$ (6.7 K). The hump observed in the heat capacity experiments above $T_c$ (7−20 K) corresponds to the increasing $\chi_{dc}T(T)$ region through the minimum (Figure 2a), suggesting short-range ferrimagnetic order in the double-chain structure extending in the $a$ direction (Figure 1a).

At present, stable radical-substituted radical cations with large $J_{intra}$ are extremely sparse. Various magnets can be designed using this strategy. In particular, it is an attractive and challenging task to design purely organic systems and also those with multiple functionality. Such studies in this and related systems are in progress.

**Acknowledgment.** We thank Iketani Science and Technology Foundation (0191002-A) for financial support. M.Ku. thanks JSPS for a Research Fellowship for Young Scientists. S.S. acknowledges Izumi Science and Technology Foundation for financial support. This work was partly supported by a Grant-in-Aid for Scientific Research (19350072) from the Ministry of Education, Sports, Culture, Science and Technology, Japan.

**Supporting Information Available:** X-ray crystallographic data (CIF), results of theoretical calculations on models I and II, and the EPR spectrum of **NNDPP**$^{\bullet+}$·$FeBr_4^-$ in frozen butyronitrile and the corresponding simulated spectrum. This material is available free of charge via the Internet at http://pubs.acs.org.

JA808093Z

(22) Blöte, H. M. J. *Physica* **1975**, *79B*, 427–466.
(23) Nakazawa, Y.; Tamura, N.; Shirakawa, N.; Shiomi, D.; Takahashi, M.; Kinoshita, M.; Ishikawa, M. *Phys. Rev. B* **1992**, *46*, 8906–8914.
(24) Pecharsky, V. K.; Miller, L. L.; Gschneidner, K. A., Jr.; Johnston, D. C. *Phys. Rev. B* **1995**, *51*, 954–961.